IJSRM
INTERNATIONAL JOURNAL OF SCIENCE AND RESEARCH METHODOLOGY
An Official Publication of Human Journals

Human Journals
Research Article
May 2019 Vol.:12, Issue:3

Effect of Media on the Properties of Monoterpene Cyclic Eucalyptol

IJSRM
INTERNATIONAL JOURNAL OF SCIENCE AND RESEARCH METHODOLOGY
An Official Publication of Human Journals

Maximiliano A. Iramain, José Ruiz Hidalgo, Silvia Antonia Brandán*

Cátedra de Química General, Instituto de Química Inorgánica, Facultad de Bioquímica. Química y Farmacia, Universidad Nacional de Tucumán, Ayacucho 471, (4000) San Miguel de Tucumán, Tucumán, Argentina.

Submission: 25 April 2019
Accepted: 30 April 2019
Published: 30 May 2019

HUMAN JOURNALS

www.ijsrm.humanjournals.com

Keywords: Eucalyptol, structural properties, force fields, vibrational analysis, DFT calculations

ABSTRACT

Structural, electronic, topological and vibrational properties of Eucalyptol have been theoretically studied in the gas phase and in acetone, chloroform, ethanol, and water solutions by using the hybrid B3LYP/6-31G* level of theory. The properties were evaluated in function of the solvent's permittivities. A higher dipole moment and lower volume values were observed for eucalyptol in water due probably to the higher permittivity. Also, higher corrected solvation energy is predicted for eucalyptol in water (-22.51 kJ/mol) in agreement with the higher volume contraction observed in this medium (-0.4 Å^3). Atomic charges reveal the most negative values on the O atoms and the most positive values on the C3 and C4 atoms. MEP surfaces of eucalyptol in all media evidence clear nucleophilic sites on the O atoms. NBO analyses show two $\Delta E_{\sigma\to\sigma^*}$ and $\Delta E_{LP\to\sigma^*}$ transitions while the AIM studies reveal two new H---H interactions which support visibly the stabilities of eucalyptol in all studied media. The gap values show a decreasing in the reactivity of eucalyptol in gas phase and mainly in chloroform and acetone solutions while in aqueous solution eucalyptol is slightly most reactive. Besides, the higher nucleophilic indexes of eucalyptol in all solvents support the characteristic nucleophilic of eucalyptol, as compared with scopolamine and tropane alkaloids. The harmonic force fields and their complete vibrational assignments of 81 normal vibration modes were performed. The predicted IR, ATR, Raman, ^{1}H- and ^{13}C-NMR and UV-visible spectra show reasonable concordance with the corresponding experimental ones.

1. INTRODUCTION

Recent studies on eucalyptol have evidenced that this natural monoterpene cyclic ether present in plants of *Eucalyptus*, *Rosmarinus* and *Salvia* among other and, also identified as 1,8-cineole or 1,8-Epoxymenthane, can be used not only in pharmaceutical preparations for external use and in clinical dentistry as gutta-percha solvents but also as high ANXA7 potentiates toxicity in hormone-refractory prostate cancer or as a potent chemopreventive agent that inhibits UVB-induced COX-2 expression by targeting AhR to suppress UVB induced skin carcinogenesis [1-8]. Therefore, eucalyptol shows other biological activities in addition to the already known anti-inflammatory and antioxidants activities [9-12]. Structurally, eucalyptol presents two fused six members rings and due to the presence of the lone pairs of electrons on the oxygen atom can form complexes, as that quinol-1,8-Epoxymenthane complex reported by Barnes [19]. On the other side, one of the most used techniques to identify since a long time this cyclic monoterpene is the vibrational spectroscopy [13-18] and, for this reason, the bands observed in the infrared and Raman spectra of eucalyptol should be completely assigned because, so far, they were not reported. Consequently, the evaluation of structural properties of eucalyptol in different media is very important taking into account the wide use of this terpene in pharmaceutical preparations and, hence, the evaluation of solvation energies of eucalyptol in different solvents is of great interest too. In this context, the aims of this work are: (i) to optimize first the structures of eucalyptol in gas phase and in the chloroform, acetone, water and ethanol solvents by using calculations derived from density functional theory (DFT) with the hybrid B3LYP/6-31G* method and the polarized continuum medium (PCM) model [20-24], (ii) to calculate the structural, electronic, topological and vibrational properties at the same level of theory, (iii) to obtain the harmonic force fields and the force constants for eucalyptol in the different media by using the scaled quantum mechanical force field (SQMFF) methodology and the Molvib program [25,26], (iv) to perform the complete vibrational assignments of experimental available infrared and Raman spectra [13,27] and, finally (v) to predict reactivities and behaviours of eucalyptol in the different media by using the frontier orbitals and some descriptors at the same level of theory [28-35]. Here, the structural properties predicted for eucalyptol in different solvents were compared with those obtained for other terpenes [36-40] and with species containing two fused cyclic rings, such as scopolamine, cocaine and tropane alkaloids and with antihistaminic cyclicine and diphenhydramine agents [41-45]. Moreover, the evaluation of pharmacological properties of eucalyptol by using some Lipinski's and

Veber's criteria is useful considering the use of this monoterpene in pharmacological preparations [46,47].

2. COMPUTATIONAL DETAILS

Figure 1 shows the molecular theoretical structure of eucalyptol together with the identification of both fused six members rings. The initial structure of eucalyptol was modeled with the *GaussView* program [48] taking into account that experimentally determined by X-ray diffraction for the Quinol-1,8-Epoxymenthane complex by Barnes [19].

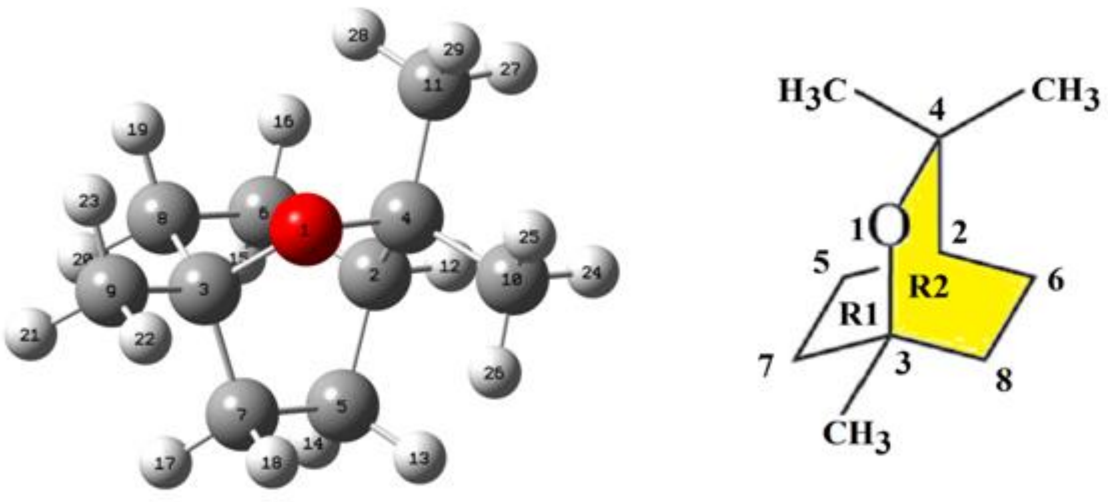

Figure 1. Theoretical molecular structures of eucalyptol, atoms labeling and identification of their rings.

The optimizations of the structure in gas phase and in the different solvents were performed by using the hybrid B3LYP/6-31G* method with the Revision A.02 of Gaussian 09 program [49] while in solution, the self-consistent reaction field (SCRF) method together with the integral equation formalism variant polarised continuum model (IEFPCM) were used to consider the solvent effects. The volumes and solvation energies in the different media were computed with the Moldraw program and the solvation model, respectively [24,50]. In addition, calculations of natural bond orbital (NBO), atoms in molecules (AIM), bond orders, molecular electrostatic potentials, stabilization energies, frontier orbitals and chemical potential (μ), electronegativity (χ), global hardness (η), global softness (S) and global electrophilicity index (ω) descriptors were carry out in order to compute the properties of eucalyptol in the different solvents at the same level of theory [51-54]. Then, with the harmonic force fields of eucalyptol calculated by using the SQMFF approach [25], the normal internal coordinates and the Molvib program [26] were performed the vibrational assignments considering potential energy distribution (PED) contributions ≥ 8-10%. Thus, the bands observed in both IR and Raman spectra could be completely assigned. Here, the ^{1}H and ^{13}C chemical shifts of eucalyptol in the different solvents also were predicted by using the Gauge-Independent Atomic Orbital (GIAO) method [55] considering as reference Trimethylsilane (TMS). Additionally, the electronic spectra in the different solvents by using Time-dependent DFT calculations (TD-DFT) with the B3LYP/6-31G* method and the Gaussian 09 program [49] were also predicted. Then, the results were compared with similar compounds.

3. RESULTS AND DISCUSSION

3.1. Properties in the gas phase and in different solvents

Calculated total energy, dipole moment and volume values for eucalyptol in the gas phase with the B3LYP/6-31G* method are compared in **Table 1** with those observed in different solvents as a function of their permittivity values. Note that the total energy values corrected by zero points vibrational energy (ZPVE) are also presented in the same table. The investigations of stationary points for the calculations in ethanol have shown an imaginary frequency value with a volume value similar to that obtained in the gas phase.

Table 1. Calculated total energies (*E*), dipole moments (μ) and volumes (V) of eucalyptol in the gas phase and in different solvents as a function of their permittivity values (ε).

B3LYP/6-31G* Method					
Medium	E (Hartrees)	ZPVE[&]	μ (D)	V (Å^3)	ε
GAS	-467.1356	-466.8691	1.30	188.5	0.00
PCM/Chloroform	-467.1459	-466.8803	1.79	188.4	4.71
PCM/Acetone	-467.1447	-466.8793	1.88	188.3	20.49
PCM/Ethanol[#]	*-467.1460*	-466.8806	*2.13*	*188.5*	24.85
PCM/Water	-467.1374	-466.8715	2.23	188.1	78.36

[#]Imaginary frequencies, [&]Zero point vibrational energy (ZPVE)

The results for chloroform and ethanol show approximately similar corrected energy values while their dipole moments present slight differences between them. However, the higher permittivity of water generates in eucalyptol a higher dipole moment (2.23 D) and a low volume in this media. Probably, the higher hydration of eucalyptol in water and the H bonds formation could justify these observations. Besides, it is clearly observed an increase in dipole moments when increasing the permittivity while the volumes decrease from eucalyptol in gas phase up to acetone, then, increase for ethanol and diminish for water. Finally, the higher corrected energy values (less negative values) are observed in the gas phase and in the water while eucalyptol is more stable in the other solvents. The volume variations observed of eucalyptol in different solvents together with corrected and uncorrected solvation energies by the total non-electrostatic terms and by zero points vibrational energy (ZPVE) with the B3LYP/6-31G* method are shown in Table 2. Analysing exhaustively the results for corrected solvation energies, it is observed a similar behaviour to that observed in the dipole moments with the permittivity values. Hence, for eucalyptol in the water, higher corrected solvation energy is predicted (-22.51 kJ/mol) in agreement with the higher volume contraction observed in this medium (-0.4 Å^3). Probably, this fact for eucalyptol in water is related to the higher energy value predicted and to high instability.

Table 2. Corrected and uncorrected solvation energies by the total non-electrostatic terms and by zero point vibrational energy (ZPVE) of eucalyptol in different solvents and their volume variations by using the B3LYP/6-31G* method.

B3LYP/6-31G* method[a]				
Solvation energy (kJ/mol)				ΔV (Å^3)
Medium	ΔG_{un}#	ΔG_{ne}	ΔG_c	
Free base				
PCM/Chloroform	-29.38	-16.64	-12.74	-0.1
PCM/Acetone	-26.75	-12.79	-13.96	-0.2
PCM/Ethanol#	-30.16	-8.99	-21.17	0.0
PCM/Water	-6.29	16.22	-22.51	-0.4

[a]This work

ΔG_{un}#= uncorrected solvation energy: defined as the difference between the total energies in aqueous solutions and the values in the gas phase.

ΔG_{ne}= total nonelectrostatic terms: due to the cavitation, dispersion and repulsion energies.

ΔG_c= corrected solvation energies: defined as the difference between the uncorrected and non-electrostatic solvation energies.

3.2. Geometrical parameters in both media

The comparisons between the calculated geometrical parameters of eucalyptol in the different media by using the B3LYP/6-31G* method with those experimental determined by X-ray diffraction for the hydroxy–cineole product obtained from cytochrome P450 monooxygenase CYP101J2 catalysed transformation of 1,8-cineole by Collis et al. [4] are summarized in **Table 3** by using the root-mean-square deviation (RMSD) values. The theoretical results in the different media show very good concordances with the predicted parameters for bond lengths between 0.013 and 0.011 Å, of 0.8º for bond angles and between 9.2 and 9.1 º for dihedral angles.

Table 3. Comparison of calculated geometrical parameters of three species of eucalyptol in the gas phase and in different solvents with the corresponding experimental ones.

Parameters	B3LYP/6-31G* Method				Experimental [b]
	Gas	Chloroform	Acetone	Water	
Bond lengths (Å)					
O1-C3	1.443	1.447	1.448	1.454	1.448(2)
O1-C4	1.452	1.457	1.457	1.464	1.466(18)
C2-C4	1.553	1.553	1.552	1.551	1.531(3)
C2-C5	1.543	1.543	1.543	1.542	1.535(3)
C2-C6	1.543	1.543	1.543	1.542	1.534(3)
C3-C7	1.542	1.541	1.541	1.539	1.526(2)
C3-C8	1.542	1.541	1.541	1.539	1.532(2)
C3-C9	1.524	1.523	1.523	1.523	1.515(2)
C4-C10	1.537	1.536	1.536	1.535	1.525(3)
C4-C11	1.537	1.536	1.536	1.535	1.523(3)
C5-C7	1.554	1.553	1.553	1.553	1.539(3)
C6-C8	1.554	1.553	1.553	1.553	1.540(3)
RMSD[b]	**0.013**	**0.012**	**0.012**	**0.011**	
Bond angles (º)					
C4-O1-C3	115.1	114.9	114.8	114.7	114.93(12)
C2-C4-O1	108.3	108.3	108.4	108.2	107.07(14)
C2-C4-C10	112.6	112.6	112.5	112.6	113.05(16)
C2-C4-C11	112.6	112.6	112.5	112.6	113.06(15)
C8-C3-O1	108.5	108.4	108.5	108.3	109.76(13)
C7-C3-O1	108.5	108.4	108.5	108.3	106.40(13)
C9-C3-O1	105.4	105.4	105.5	105.6	106.18(14)
C10-C4-O1	107.1	107.1	107.2	107.1	106.51(13)
C11-C4-O1	107.1	107.1	107.2	107.1	107.90(15)
C2-C6-C8	108.6	108.6	108.6	108.6	108.51(14)
C6-C2-C4	109.8	109.9	109.9	109.9	110.26(16)
C6-C2-C5	107.0	107.1	107.1	107.1	107.20(16)
C6-C8-C3	109.4	109.4	109.4	109.5	109.29(14)
C7-C3-C8	109.8	109.9	109.8	110.0	109.91(14)
C7-C3-C9	112.1	112.1	112.0	112.1	112.35(16)
C10-C4-C11	108.5	108.5	108.5	108.6	108.91(16)
RMSD[b]	**0.8**	**0.8**	**0.8**	**0.8**	
Dihedral angles (º)					
C3-O1-C4-C10	-121.8	-121.8	-121.8	-121.7	-134.02(16)
C3-O1-C4-C11	121.8	121.8	121.7	121.7	109.18(16)
C4-O1-C3-C7	59.6	59.6	59.6	59.6	68.89(16)
C4-O1-C3-C8	-59.6	-59.6	-59.6	-59.6	-50.00(18)
C4-O1-C3-C9	-179.9	-179.9	-179.9	-179.9	-171.24(15)
O1-C4-C2-C5	-58.7	-58.8	-58.8	-58.9	-51.77(18)
O1-C4-C2-C6	58.7	58.8	58.8	58.9	65.78(18)
O1-C3-C8-C6	60.2	60.3	60.2	60.4	63.37(18)
RMSD[b]	**9.2**	**9.1**	**9.1**	**9.1**	

[a]This work, [b]Ref [11]

Low RMSD values are evidenced for eucalyptol in all media but, in particular, in gas phase little differences in the bond lengths and dihedral angles. Obviously, these structures of eucalyptol in the different media can clearly be used to perform the corresponding vibrational analyses.

3.3. Charges, molecular electrostatic potential and bond orders studies

The evaluation of charges, molecular electrostatic potentials (MEP) and bond orders for eucalyptol in the different media are of great importance considering the presence of an O atom and a bicyclic ring in its structure and taking into account their wide pharmacological properties, as was observed for some alkaloids with similar fused rings [41-43,45]. Hence, atomic Mulliken, Merz-Kollman (MK) and NPA charges together with the MEP values and bond orders were computed for eucalyptol in all media at the same level of theory. Here, the results are presented in **Table 4** only for the first ten atoms which present the higher variations. Obviously, the values in ethanol were not presented due to the imaginary frequency obtained during the optimization. The behaviors of each charge on those ten atoms of eucalyptol in the four media are observed in **Figure 2**. The three charges present approximately the same variations although the values among them are very different, as can be seen in the figure. Thus, on the O atoms are observed the most negative MK, Mulliken and NPA charges while the most positive values are observed on the C3 and C4 atoms. Besides, on the C2, C5, C6, C7, and C8 have observed approximately the same MK charges but the values are completely different from the Mulliken and NPA values.

Table 4. Mulliken, Merz-Kollman and NPA charges (a.u.), molecular electrostatic potentials (MEP) (a.u.) and bond orders, expressed as Wiberg indexes of eucalyptol in the gas phase and in different solvents by using B3LYP/6-31G* calculations.

	GAS					Chloroform				
Atoms	MK	Mulliken	NPA	MEP	BO	MK	Mulliken	NPA	MEP	BO
1 O	-0.572	-0.549	-0.614	-22.339	1.980	-0.573	-0.551	-0.614	-22.340	1.978
2 C	-0.078	-0.110	-0.282	-14.741	3.944	-0.067	-0.110	-0.282	-14.741	3.944
3 C	0.551	0.312	0.280	-14.693	3.918	0.549	0.313	0.279	-14.693	3.918
4 C	0.770	0.339	0.282	-14.690	3.922	0.766	0.341	0.281	-14.690	3.923
5 C	-0.120	-0.286	-0.460	-14.746	3.900	-0.127	-0.286	-0.460	-14.746	3.900
6 C	-0.120	-0.286	-0.460	-14.746	3.900	-0.127	-0.286	-0.460	-14.746	3.900
7 C	-0.144	-0.272	-0.483	-14.750	3.901	-0.140	-0.272	-0.483	-14.750	3.901
8 C	-0.144	-0.272	-0.483	-14.750	3.901	-0.140	-0.272	-0.483	-14.750	3.901
9 C	-0.506	-0.458	-0.677	-14.758	3.847	-0.504	-0.458	-0.677	-14.758	3.847
10 C	-0.559	-0.451	-0.685	-14.760	3.852	-0.563	-0.452	-0.685	-14.759	3.852
11 C	-0.558	-0.451	-0.685	-14.760	3.852	-0.563	-0.452	-0.685	-14.759	3.852
	Acetone					Water				
Atoms	MK	Mulliken	NPA	MEP	BO	MK	Mulliken	NPA	MEP	BO
1 O	-0.572	-0.552	-0.614	-22.340	1.978	-0.572	-0.555	-0.615	-22.341	1.974
2 C	-0.064	-0.110	-0.282	-14.741	3.944	-0.062	-0.109	-0.282	-14.741	3.944
3 C	0.549	0.313	0.279	-14.693	3.918	0.546	0.313	0.279	-14.693	3.919
4 C	0.764	0.341	0.281	-14.690	3.923	0.762	0.340	0.281	-14.690	3.924
5 C	-0.129	-0.286	-0.460	-14.746	3.900	-0.130	-0.286	-0.459	-14.746	3.900
6 C	-0.129	-0.286	-0.460	-14.746	3.900	-0.130	-0.286	-0.459	-14.746	3.900
7 C	-0.138	-0.272	-0.483	-14.750	3.901	-0.138	-0.272	-0.483	-14.750	3.901
8 C	-0.139	-0.272	-0.483	-14.750	3.901	-0.138	-0.272	-0.483	-14.750	3.901
9 C	-0.499	-0.458	-0.677	-14.758	3.847	-0.496	-0.458	-0.677	-14.758	3.847
10 C	-0.565	-0.452	-0.686	-14.759	3.852	-0.566	-0.451	-0.685	-14.759	3.851
11 C	-0.566	-0.452	-0.686	-14.759	3.852	-0.566	-0.451	-0.685	-14.759	3.851

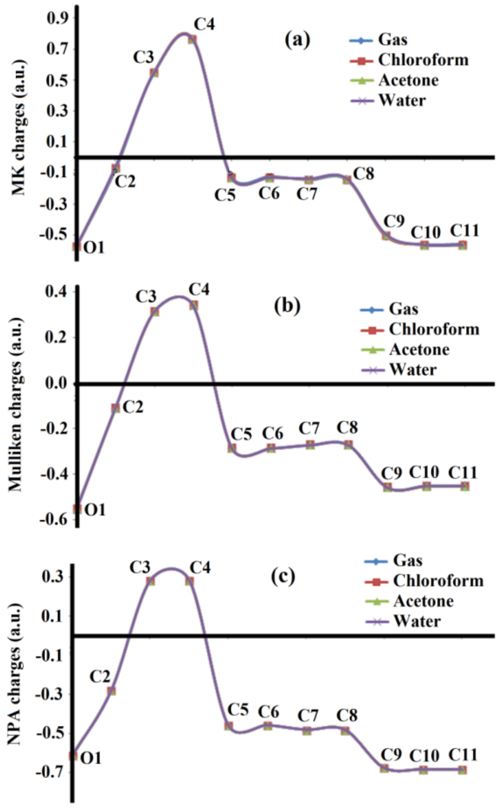

Figure 2. Calculated MK, Mulliken, and NPA charges on ten atoms of eucalyptol in the four media by using the B3LYP/6-31G* method.

I now we analysed the molecular electrostatic potentials from Table 4, obviously, on the O atoms are observed the most negative values while on the C the less negative values being the tendency: O > C > Hand, moreover, the same values are observed approximately on all atoms in the different media. However, when the mapped MEP surfaces of eucalyptol in the different media are graphed in **Figure 3** differences in the colorations can clearly be seen. Thus, strong red colors are observed on the O atoms indicative of nucleophilic sites while on remaining atoms are observed green colors typical of inert regions. There are not different among the red colorations.

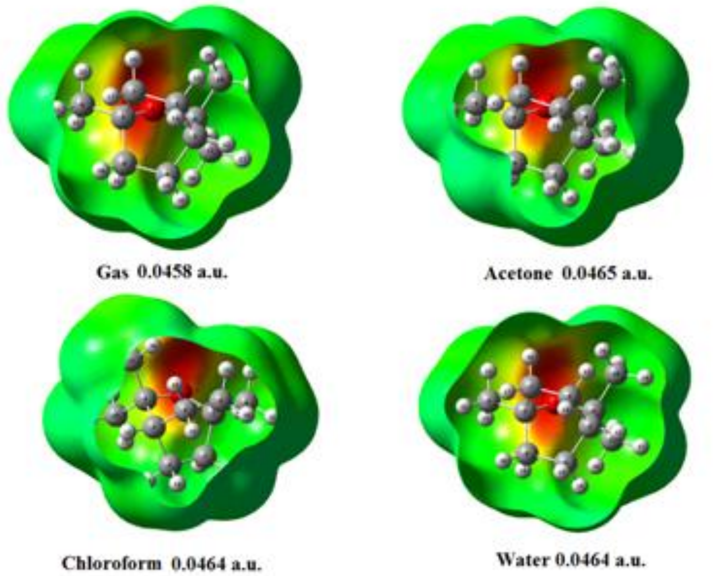

Figure 3. Calculated electrostatic potential surfaces on the molecular surfaces of eucalyptol in different media. Color ranges are indicated in units a.u. B3LYP functional and 6-31G* basis set. Isodensity value of 0.005.

The bond orders (BO), expressed as Wiberg indexes were also predicted for eucalyptol in the different media. The results are presented in Table 4 and show a similar tendency to the MEP values because the higher values are observed in the C atoms while the lower values in H atoms. Here, the C2 atoms present the higher BO values while the lower values are observed in the C9 atoms. The O atoms show the lower value in water and the higher one in the gas phase, as compared with the other media.

3.4. Donor-acceptor energy interactions

The stabilities of eucalyptol in the different media main were studied by using the donor-acceptor energy interactions calculating the second order perturbation theory analysis of Fock matrix by using NBO Basis with the NBO program [52]. Then, the main delocalization energies by using the B3LYP/6-31G* method are summarized in **Table 5**. Here, two different interactions from bonding C-H orbitals to antibonding C-O orbitals ($\Delta E_{\sigma\rightarrow\sigma^*}$) and from lone pairs of O1 atoms to antibonding C-C orbitals ($\Delta E_{LP\rightarrow\sigma^*}$) can be observed in the table. In general, when the total energies are computed the higher values are observed in the gas phase and in acetone solvent while the lower value it is observed in water. Hence, these studies suggest that eucalyptol is slightly stable in the four media.

Table 5. Main delocalization energies (in kJ/mol) of eucalyptol in the gas phase and in different solvents by using B3LYP/6-31G* calculations.

Delocalization	B3LYP/6-31G*[a]			
	Gas	Chloroform	Acetone	Water
*σC7-H17→ σ*O1-C3*	17.01	17.18	17.26	17.47
*σC8-H20→ σ*O1-C3*	17.01	17.18	17.26	17.47
*σC9-H21→ σ*O1-C3*	17.47	17.72	17.85	18.27
*σC10-H24→ σ*O1-C4*	17.05	17.31	17.39	17.72
*σC11-H27→ σ*O1-C4*	17.05	17.31	17.39	17.72
$\Delta E_{\sigma\to\sigma^*}$	**85.61**	**86.69**	**87.15**	**88.66**
*LP(2)O1→σ*C3-C7*	23.58	23.12	23.12	22.32
*LP(2)O1→ σ*C3-C8*	23.58	23.12	23.12	22.32
*LP(2)O1→ σ*C4-C10*	19.40	19.06	19.10	18.48
*LP(2)O1→ σ*C4-C11*	19.40	19.06	19.10	18.52
$\Delta E_{LP\to\sigma^*}$	**85.94**	**84.35**	**84.44**	**81.64**
ΔE_{TOTAL}	**171.55**	**171.05**	**171.59**	**170.29**

[a]This work

3.5. Topological properties

The topological parameters, such as the electron density, $\rho(r)$, the Laplacian values, $\nabla^2\rho(r)$, the eigenvalues $(\lambda 1, \lambda 2, \lambda 3)$ of the Hessian matrix and, the $|\lambda 1|/\lambda 3$ ratio are very useful to investigate different interactions, such as ionic, covalent and hydrogen bonds interactions, as suggested by the Bader's theory [53]. Hence, if those parameters calculated in the bond critical points (BCPs) and ring critical points (RCPs) show that $\lambda 1/\lambda 3 < 1$ and $\nabla^2\rho(r) > 0$ the interaction is ionic or highly polar covalent (closed-shell interaction). Then, the presence of inter or intra-molecular interactions can easily increase the stability of a species. In this work, those parameters were calculated for eucalyptol in the different media by using the B3LYP/6-31G* method and the AIM2000 program [54] which are presented in **Table 6**. Eucalyptol reveals in each medium the formation of two different H26---H13 and H28---H16 interactions which generate two new RCPs, RCPN1 and RCPN2, as can be seen in **Figure 4**. Here, RCP1, RCP2, and RCP3 are the RCPs of the two fused rings and of others formed as a consequence of bicyclic ring.

Note that for eucalyptol in all media the electron density and the Laplacian values observed in the H---H interactions and their corresponding RCPN present practically the same values in the four media. These facts suggest that both critical points have approximately the same characteristics. Besides, the distances between the H atoms of H---H interactions are the same in chloroform and acetone but in the gas phase and in water present the lower values. These results practically don't show significant differences among the topological parameters and, obviously, support the stabilities of eucalyptol in all studied media.

Table 6. Analysis of the Bond Critical Points (BCPs) and Ring critical point (RCPs) of eucalyptol in the gas phase and in different solvents by using the B3LYP/6-31G* method.

B3LYP/6-31G* Method							
GAS PHASE							
Parameter[#]	H26---H13	RCPN1	H28---H16	RCPN2	RCP1	RCP2	RCP3
ρ(r)	0.0107	0.0107	0.0107	0.0107	0.0220	0.0220	0.0215
$\nabla^2\rho(r)$	0.0464	0.0482	0.0464	0.0482	0.1281	0.1281	0.1337
λ1	-0.0088	-0.0083	-0.0088	-0.0083	-0.0074	-0.0074	-0.0043
λ2	-0.0015	0.0016	-0.0015	0.0016	0.0381	0.0381	0.0305
λ3	0.0567	0.0549	0.0567	0.0549	0.1054	0.1054	0.1074
|λ1|/λ3	0.1552	0.1512	0.1552	0.1512	0.0702	0.0702	0.0400
Distances (Å)	2.159		2.159				
Chloroform							
Parameter[#]	H26---H13	RCPN1	H28---H16	RCPN2	RCP1	RCP2	RCP3
ρ(r)	0.0106	0.0106	0.0106	0.0106	0.0219	0.0219	0.0215
$\nabla^2\rho(r)$	0.0464	0.0479	0.0464	0.0478	0.1356	0.1356	0.1337
λ1	-0.0087	-0.0083	-0.0087	-0.0083	-0.0073	-0.0073	-0.0045
λ2	-0.0013	0.0013	-0.0013	0.0013	0.0378	0.0378	0.0310
λ3	0.0564	0.0549	0.0564	0.0549	0.1051	0.1051	0.1071
|λ1|/λ3	0.1543	0.1512	0.1543	0.1512	0.0695	0.0695	0.0420
Distances (Å)	2.161		2.161				
Acetone							
Parameter[#]	H26---H13	RCPN1	H28---H16	RCPN2	RCP1	RCP2	RCP3
ρ(r)	0.0107	0.0107	0.0107	0.0107	0.0219	0.0219	0.0215
$\nabla^2\rho(r)$	0.0465	0.0479	0.0465	0.0479	0.1356	0.1356	0.1338
λ1	-0.0087	-0.0083	-0.0087	-0.0083	-0.0073	-0.0073	-0.0045
λ2	-0.0012	0.0013	-0.0012	0.0013	0.0376	0.0376	0.0311
λ3	0.0564	0.0550	0.0564	0.0550	0.1053	0.1053	0.1072
|λ1|/λ3	0.1543	0.1509	0.1543	0.1509	0.0693	0.0693	0.0420
Distances (Å)	2.161		2.161				
Water							
Parameter[#]	H26---H13	RCPN1	H28---H16	RCPN2	RCP1	RCP2	RCP3
ρ(r)	0.0107	0.0107	0.0107	0.0107	0.0218	0.0218	0.0215
$\nabla^2\rho(r)$	0.0466	0.0466	0.0466	0.0466	0.1348	0.1348	0.1337
λ1	-0.0088	-0.0088	-0.0088	-0.0088	-0.0072	-0.0072	-0.0049
λ2	-0.0015	-0.0015	-0.0015	-0.0015	0.0376	0.0376	0.0321
λ3	0.0569	0.0569	0.0569	0.0569	0.1044	0.1044	0.1064
|λ1|/λ3	0.1547	0.1547	0.1547	0.1547	0.0690	0.0690	0.0461
Distances (Å)	2.157		2.158				

[#]The properties are expressed in a.u.

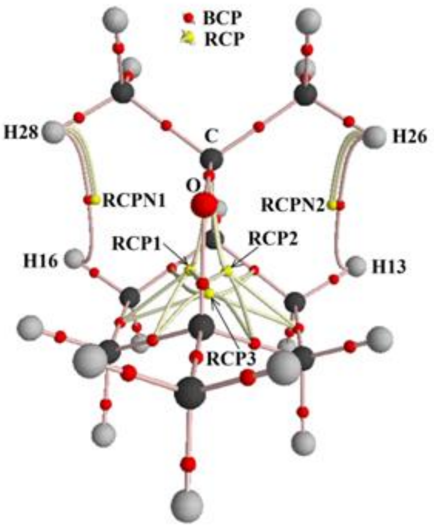

Figure 4. Molecular graphic for eucalyptol in gas phase showing the geometry of all their bond critical points (BCPs) and ring critical points (RCPs) by using the B3LYP/6-31G* method.

3.6. Reactivities and behaviours in different media

The above studies have demonstrated that the behavior of eucalyptol in the different solvent is practically independent of their permittivity's values for which few differences are observed in the properties. In this section, in order to investigate the reactivities and behaviors of this cyclic monoterpene ether in different media, the frontier orbitals were employed to compute the gap values of the corresponding differences between these orbitals, as suggested by Parr and Pearson [28]. Then, with these values were later calculated the chemical potential (μ), electronegativity (χ), global hardness (η), global softness (S), global electrophilicity index (ω) and global nucleophilicity index (E) descriptors [29-40]. These results can be seen in **Table 7** compared with the corresponding to species containing bicyclic rings such as free base species of scopolamine and tropane alkaloids [41,43]. **Figure 5** shows clearly the differences among the descriptors of two compared species. Analysing first the gap values for eucalyptol in all media it is observed that the presence of an O atom linked to a bicyclic ring in eucalyptol increase the difference between the frontier HOMO and LUMO orbitals decreasing the reactivities of eucalyptol in gas phase and mainly in chloroform and acetone solutions while in aqueous solution eucalyptol is slightly most reactive. However, the difference with scopolamine and tropane is most significant evidencing that scopolamine and tropane are most reactive than eucalyptol in different media. Here, the presence of N atoms and different bicyclic rings in the two compared species could clearly justify the differences with eucalyptol. When the descriptors are compared among them, Fig. 5 shows that eucalyptol in different media present higher global hardness (η) and the most negative global nucleophilicity index (E) than scopolamine and tropane alkaloids while scopolamine has higher electronegativity (χ) and global electrophilicity index (ω). Here, the presence of additional groups in scopolamine clearly increases the electrophilicity index as compared to eucalyptol but, this monoterpene ether is most nucleophilic in all media, as revealed by the MEP surfaces analyzed in section 3.3. Evidently, these studies of frontier orbitals support the characteristics of eucalyptol as a powerful nucleophile against reacting with potential biological electrophiles.

Table 7. Frontier molecular HOMO and LUMO orbitals and gap values of eucalyptol in the gas phase and in different solvents by using the B3LYP/6-31G* level of theory.

	Eucalyptol[a]				Scopolamine[b]	Tropane[c]
Orbital	Gas	Chloroform	Acetone	Water	Gas	Gas
HOMO	-6.2396	-6.2369	-6.2396	-6.2314	-5.765	-5.4945
LUMO	1.8613	1.8558	1.8504	1.8477	-0.3646	2.0561
|GAP|	8.1009	8.0927	8.0900	8.0791	5.4004	7.5506
			Descriptors			
Descriptor	Gas	Chloroform	Acetone	Water	Gas	Gas
χ	-4.0505	-4.0464	-4.0450	-4.0396	-2.462	-3.4123
μ	-2.1892	-2.1906	-2.1946	-2.1919	-2.9289	-2.1787
η	4.0505	4.0464	4.0450	4.0396	2.462	3.4123
S	0.1234	0.1236	0.1236	0.1238	0.2031	0.1465
ω	0.5916	0.5929	0.5953	0.5946	1.7421	0.6955
E	-8.8670	-8.8637	-8.8772	-8.8541	-7.2107	-7.4343

[a]This work, [b]From Ref [43], [c]From Ref [41]

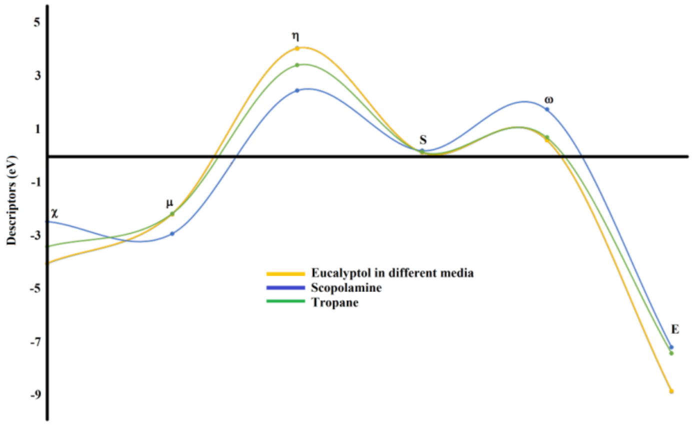

Figure 5. Calculated descriptors values of eucalyptol in different media compared with the corresponding to the free base species of scopolamine and tropane alkaloids in the gas phase by using the B3LYP/6-31G* method.

3.7. Vibrational study

The structure's eucalyptol in all media was optimized with C_1 symmetries by using the hybrid B3LYP/6-31G* method. In the four media, 81 normal vibration modes are expected in both infrared and Raman spectra and all vibration modes present activities in both infrared and Raman spectra. **Figures 6** and **7** show the experimental available infrared and Raman spectra of eucalyptol taken from References [13] and [27], respectively which are compared with the corresponding predicted in the gas phase and in acetone, water and chloroform by using the hybrid B3LYP/6-31G* level of theory. The experimental attenuated total reflectance (ATR) spectrum of eucalyptol taken from Ref [27] can be seen in **Figure 8** compared with the predicted for monomer and dimer ones of eucalyptol in the gas phase by using the same level of theory. Good correlations can be observed among all the spectra especially when the dimeric species is considered because the intensities of bands in the 1500-500 cm^{-1} region are significantly increased in accordance with the experimental ones. Here, the predicted Raman spectra expressed in activities were changed to intensities employing equations suggested from the literature [56,57]. To perform the vibrational assignments of eucalyptol in the four media the normal internal coordinates and suggested scale factors were used together with the SQMFF methodology and the Molvib program to acquire the harmonic force fields [25,26,58].

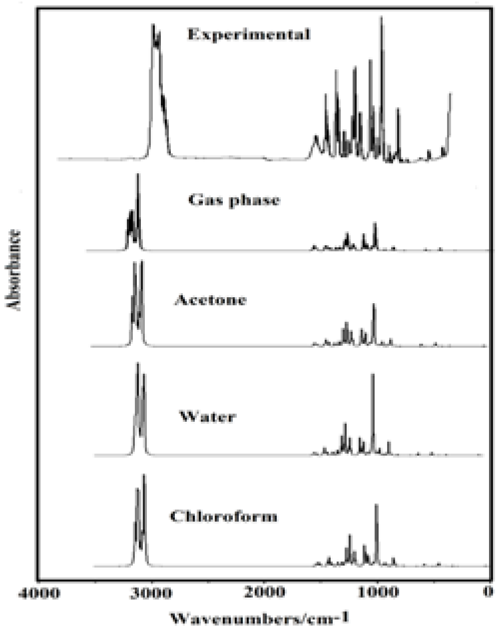

Figure 6. The experimental infrared spectrum of eucalyptol compared with the corresponding predicted in the gas phase and in acetone, water, and chloroform solutions by using B3LYP/6-31G* level of theory.

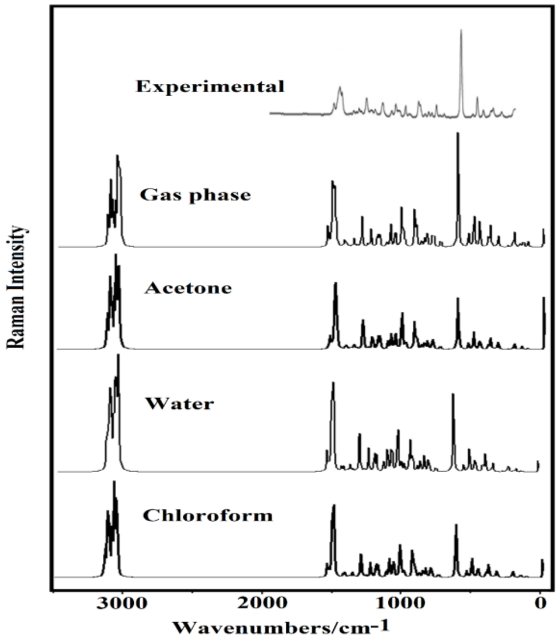

Figure 7. Experimental Raman spectrum of eucalyptol compared with the corresponding predicted in the gas phase and in acetone, water, and chloroform solutions by using B3LYP/6-31G* level of theory.

Here, only potential energy distribution (PED) contributions between 9 and 10 % were used in the assignments. In **Table 8** are summarized observed and calculated wavenumbers for eucalyptol in the different media and their corresponding assignments. Here, a very important observation is that in general all vibration modes are predicted strongly coupled with other ones. Then, some assignments for the most important groups are discussed.

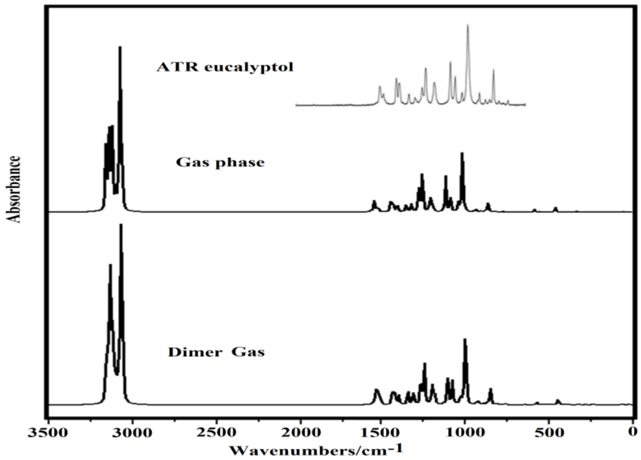

Figure 8. Experimental attenuated total reflectance spectrum of eucalyptol compared with the corresponding predicted in the gas phase for monomer and dimer by using B3LYP/6-31G* level of theory.

Table 8. Observed and calculated wavenumbers (cm^{-1}) and assignments of eucalyptol in the gas phase and in different solvents.

Experimental			B3LYP/6-31G* Method[a]							
			Gas		Chloroform		Acetone		Water	
IR[c]	ATR[d]	Raman[d]	SQM[b]	Assignments[a]	SQM[b]	Assignments[a]	SQM[b]	Assignments[a]	SQM[b]	Assignments[a]
3005sh			3013	ν_aCH_3(C11)	3008	ν_aCH_3(C10)	3007	ν_aCH_3(C10)	3009	ν_aCH_3(C10)
			3012	ν_aCH_3(C10)	3008	ν_aCH_3(C11)	3007	ν_aCH_3(C11)	3009	ν_aCH_3(C11)
			2998	ν_aCH_3(C9)	2993	ν_aCH_3(C9)	2992	ν_aCH_3(C9)	2997	ν_aCH_3(C9)
			2996	ν_aCH_3(C9)	2988	ν_aCH_3(C9)	2986	ν_aCH_3(C9)	2989	ν_aCH_3(C11)
			2994	ν_aCH_3(C10)	2987	ν_aCH_3(C10)	2985	ν_aCH_3(C10)	2988	ν_aCH_3(C9)
2985sh			2986	ν_aCH_3(C11)	2980	ν_aCH_3(C11)	2978	ν_aCH_3(C11)	2983	ν_aCH_3(C10)
			2980	ν_aCH_2(C6)	2978	ν_aCH_2(C6)	2977	ν_aCH_2(C5)	2981	ν_aCH_2(C5)
2971vs			2976	ν_aCH_2(C5)	2975	ν_aCH_2(C5)	2974	ν_aCH_2(C6)	2978	ν_aCH_2(C6)
			2959	ν_aCH_2(C8)	2959	ν_aCH_2(C8)	2958	ν_aCH_2(C8)	2963	ν_aCH_2(C8)
2946s			2957	ν_aCH_2(C7)	2956	ν_aCH_2(C7)	2956	ν_aCH_2(C7)	2961	ν_aCH_2(C7)
			2943	ν_sCH_2(C5)	2945	νC2-H12	2945	νC2-H12	2949	νC2-H12
			2932	νC2-H12 ν_sCH_3(C9)	2932	ν_sCH_2(C8)	2932	ν_sCH_2(C8)	2936	νC2-H12 ν_sCH_2(C5)
			2931	ν_sCH_2(C6)	2931	ν_sCH_2(C6) ν_sCH_2(C5)	2931	ν_sCH_2(C5) ν_sCH_2(C6)	2936	ν_sCH_2(C6) ν_sCH_2(C5)
2923s			2929	ν_sCH_3(C11)	2928	ν_sCH_3(C10)	2926	ν_sCH_3(C10)	2931	ν_sCH_3(C11)
2885m			2926	νC2-H12 ν_sCH_3(C9)	2925	ν_sCH_3(C9) ν_sCH_2(C5)	2924	ν_sCH_3(C9) ν_sCH_2(C6)	2929	ν_sCH_3(C9) ν_sCH_2(C7)
2876m			2924	ν_sCH_3(C10)	2922	ν_sCH_3(C11)	2921	ν_sCH_3(C11)	2926	ν_sCH_3(C10)
2857w			2922	ν_sCH_2(C8)	2920	ν_sCH_3(C9)	2920	ν_sCH_3(C9)	2924	ν_sCH_2(C8)

			2919	$\nu_{s}CH_{2}$(C7) $\nu_{s}CH_{2}$(C8) $\nu_{s}CH_{2}$(C7)	2919	$\nu_{s}CH_{2}$(C7)	2919	$\nu_{s}CH_{2}$(C7)	2923	$\nu_{s}CH_{3}$(C9) $\nu_{s}CH_{2}$(C8)
1553w		1487m	1492	δCH_{2}(C5)	1478	δCH_{2}(C5)	1474	δCH_{2}(C5) δCH_{2}(C6)	1473	δCH_{2}(C5) δCH_{2}(C6)
1487w			1474	δCH_{2}(C6)	1464	δCH_{2}(C6)	1462	δCH_{2}(C6) δCH_{2}(C5)	1462	δCH_{2}(C6) δCH_{2}(C5)
1470m			1470	$\delta_{a}CH_{3}$(C11) $\delta_{a}CH_{3}$(C10)	1455	$\delta_{a}CH_{3}$(C11) $\delta_{a}CH_{3}$(C10)	1452	$\delta_{a}CH_{3}$(C11)	1451	$\delta_{a}CH_{3}$(C11) $\delta_{a}CH_{3}$(C10)
1450w			1463	$\delta_{a}CH_{3}$(C9)	1448	$\delta_{a}CH_{3}$(C10) $\delta_{a}CH_{3}$(C11)	1445	$\delta_{a}CH_{3}$(C11) $\delta_{a}CH_{3}$(C10)	1446	$\delta_{a}CH_{3}$(C11) $\delta_{a}CH_{3}$(C10)
	1459m	1457sh	1460	$\delta_{a}CH_{3}$(C11) $\delta_{a}CH_{3}$(C10)	1441	$\delta_{a}CH_{3}$(C10) $\delta_{a}CH_{3}$(C11)	1438	$\delta_{a}CH_{3}$(C10)	1437	$\delta_{a}CH_{3}$(C11) $\delta_{a}CH_{3}$(C10)
			1453	$\delta_{a}CH_{3}$(C9) $\delta_{a}CH_{3}$(C10)	1441	$\delta_{a}CH_{3}$(C9)	1437	$\delta_{a}CH_{3}$(C9)	1436	$\delta_{a}CH_{3}$(C9)
		1449s	1448	$\delta_{a}CH_{3}$(C9)	1434	δCH_{2}(C8) δCH_{2}(C7)	1431	δCH_{2}(C8) δCH_{2}(C7)	1431	$\delta_{a}CH_{3}$(C11) $\delta_{a}CH_{3}$(C10)
			1447	δCH_{2}(C7)	1433	$\delta_{a}CH_{3}$(C9)	1430	$\delta_{a}CH_{3}$(C9) δCH_{2}(C7)	1431	δCH_{2}(C8) δCH_{2}(C7)
1442sh	1440w		1441	$\delta_{a}CH_{3}$(C11) $\delta_{a}CH_{3}$(C10)	1432	$\delta_{a}CH_{3}$(C11) $\delta_{a}CH_{3}$(C10)	1430	$\delta_{a}CH_{3}$(C11) $\delta_{a}CH_{3}$(C10)	1429	$\delta_{a}CH_{3}$(C9) δCH_{2}(C7)
1426w		1435s	1435	δCH_{2}(C8)	1427	δCH_{2}(C7) δCH_{2}(C8)	1425	$\delta_{a}CH_{3}$(C9)	1424	$\delta_{a}CH_{3}$(C9)
1377s			1380	$\delta_{s}CH_{3}$(C10)	1371	$\delta_{s}CH_{3}$(C10) $\delta_{s}CH_{3}$(C11)	1369	wagCH_{2}(C8) wagCH_{2}(C7)	1373	$\delta_{s}CH_{3}$(C10) $\delta_{s}CH_{3}$(C11)
1374sh		1378vw	1375	wagCH_{2}(C8)	1370	wagCH_{2}(C8) wagCH_{2}(C7)	1369	$\delta_{s}CH_{3}$(C10)	1371	wagCH_{2}(C8) wagCH_{2}(C7)
	1370s		1371	$\delta_{s}CH_{3}$(C9)	1361	wagCH_{2}(C6)	1360	wagCH_{2}(C6)	1362	wagCH_{2}(C6)
1364m			1361	wagCH_{2}(C6)	1358	$\delta_{s}CH_{3}$(C11) $\delta_{s}CH_{3}$(C10)	1357	$\delta_{s}CH_{3}$(C11)	1359	$\delta_{s}CH_{3}$(C10) $\delta_{s}CH_{3}$(C11)
1358m	1354m	1356w	1361	$\delta_{s}CH_{3}$(C11)	1353	$\delta_{s}CH_{3}$(C9)	1351	$\delta_{s}CH_{3}$(C9)	1352	$\delta_{s}CH_{3}$(C9)
1337w	1335w	1339vw	1344	wagCH_{2}(C5) ρ’C2-H12	1341	wagCH_{2}(C5) ρ’C2-H12	1341	wagCH_{2}(C5)	1343	wagCH_{2}(C5) ρ’C2-H12
1331sh		1322w	1324	wagCH_{2}(C7)	1321	wagCH_{2}(C7) wagCH_{2}(C8)	1321	wagCH_{2}(C7) wagCH_{2}(C8)	1324	wagCH_{2}(C7) wagCH_{2}(C8)
1309w	1301w	1307w	1312	ρC2-H12 τR_{2}(A2)	1305	τR_{2}(A2) ρC2-H12	1304	τR_{2}(A2) ρC2-H12	1307	τR_{2}(A2) ρC2-H12
1277sh			1282	ρCH_{2}(C8) ρCH_{2}(C7)	1271	τR_{1}(A1) τR_{2}(A2)	1271	ρCH_{2}(C8) ρCH_{2}(C7)	1271	ρCH_{2}(C8) ρCH_{2}(C7)
1273w	1270w	1272s	1275	τR_{1}(A1) τR_{2}(A2)	1271	ρCH_{2}(C8) ρCH_{2}(C7)	1270	τR_{1}(A1) τR_{2}(A2)	1270	τR_{1}(A1) τR_{2}(A2)
1245sh	1238sh	1241w	1236	τR_{1}(A1)	1232	τR_{1}(A1)	1231	τR_{1}(A1)	1233	ρ'CH_{3}(C11)
1236w	1233m		1235	τR_{3}(A2)	1229	τR_{3}(A2)	1228	τR_{3}(A2)	1231	τR_{3}(A2)
1215s	1211s	1218w	1219	ρC2-H12 ρCH_{2}(C5)	1205	ρC2-H12 ρCH_{2}(C5)	1204	ρC2-H12 ρCH_{2}(C5)	1207	ρC2-H12 ρCH_{2}(C5)

			1202	τR_1(A1)	1195	τR_1(A1)	1195	τR_1(A1)	1198	τR_1(A1)
1170m	1166m	1169m	1161	τR_2(A1) τR_3(A2)	1153	τR_2(A1)	1153	τR_2(A1)	1151	τR_1(A1) τR_3(A2)
1163sh	1159sh	1158sh	1154	τR_1(A1) τR_2(A2)	1150	τR_1(A1) τR_2(A2)	1149	τR_1(A1) τR_2(A2)	1151	τR_2(A2) τR_1(A1)
			1152	νC3-C9	1148	νC3-C9	1148	νC3-C9	1148	νC3-C9
1110vw	1108vw	1108w	1108	ρ'CH_3(C9) ρCH_2(C6)	1099	ρ'CH_3(C9) ρCH_2(C6)	1098	ρ'CH_3(C9) ρCH_2(C6)	1101	ρ'CH_3(C9) ρCH_2(C6)
1080s	1078s	1083m	1076	ρCH_3(C9)	1067	ρCH_3(C9)	1065	ρCH_3(C9)	1064	ρCH_3(C9)
1054m	1055m	1064w	1042	νC2-C6 νC2-C5 νC6-C8 νC5-C7	1039	νC2-C6 νC2-C5 νC6-C8 νC5-C7	1039	νC2-C6 νC2-C5 νC6-C8 νC5-C7	1042	νC2-C6 νC5-C7
1015w	1016w	1017m	1022	τR_1(A1) τR_2(A1)	1018	τR_1(A1) τR_2(A1)	1017	τR_1(A1) τR_2(A1)	1018	τR_1(A1) τR_2(A1)
985vs	986vs	992w	996	τR_2(A1) τR_3(A2)	997	ρCH_3(C10) ρCH_3(C11) ρ'CH_3(C11)	997	ρCH_3(C10) ρCH_3(C11) ρ'CH_3(C10)	1000	ρCH_3(C10) ρCH_3(C11) ρ'CH_3(C11) ρ'CH_3(C10)
985vs		980sh	995	ρCH_3(C11) ρ'CH_3(C10) ρCH_3(C10) ρ'CH_3(C11)	991	τR_2(A1) τR_3(A2)	990	τR_3(A2) τR_3(A2)	991	τR_2(A1) τR_1(A1)
975sh	969sh		973	νO1-C3	962	νO1-C3	960	νO1-C3	954	τR_1(A1) τR_2(A1)
	933sh	932m	956	τR_1(A1) τR_2(A1)	952	τR_1(A1) τR_2(A1)	952	τR_1(A1) R_2(A1)	950	νO1-C3
929vw	923w	920sh	913	νC2-C4	912	νC2-C4	912	νC2-C4	914	νC2-C4
920w			909	νC4-C10 νC4-C11	910	νC4-C10 ρ'CH_3(C10)	909	ρ'CH_3(C11) νC4-C10	913	νC4-C10
889vw	891w	888w	895	τR_1(A1)	892	τR_1(A1)	891	τR_1(A1)	891	τR_1(A1)
	868w		876	τR_2(A1) τR_3(A2)	875	τR_2(A1) τR_3(A2)	876	τR_2(A1) τR_3(A2)	878	τR_2(A1) τR_3(A2)
866w		865w	862	τR_2(A2) τR_3(A1)	862	τR_2(A2) τR_3(A1)	861	τR_2(A2) τR_3(A1)	861	τR_2(A2) τR_3(A1)
844m	848s	843w	835	νC2-C6 νC2-C5	832	νC4-C11	832	νC4-C11	832	νC2-C5 νC4-C11
814w	818w	814m	819	νO1-C4	813	νO1-C4	813	νO1-C4	810	νO1-C4
791vw	792w	790w	777	τR_1(A1)	774	τR_1(A1)	774	τR_1(A1) τR_2(A1)	774	τR_1(A1)
764vw	777sh	764w	733	τwCH_2(C5) τwCH_2(C6) τwCH_2(C7) τwCH_2(C8)	731	τwCH_2(C5) τwCH_2(C6) τwCH_2(C7) τwCH_2(C8)	731	τwCH_2(C5) τwCH_2(C6) τwCH_2(C7) τwCH_2(C8)	730	τwCH_2(C5) τwCH_2(C7) τwCH_2(C8)

	731vw	728	νC3-C8 νC3-C7	728	νC3-C8 νC3-C7	728	νC3-C8 νC3-C7	727	νC3-C8 νC3-C7
649vw	651vs	625	νC2-C4 τR$_3$(A2)	624	νC2-C4 τR$_3$(A2)	624	νC2-C4 τR$_3$(A2)	624	νC2-C4 τR$_3$(A2)
576vw	575w	563	τR$_1$(A1) τR$_2$(A2)	563	τR$_1$(A1) τR$_2$(A2)	563	τR$_1$(A1) τR$_2$(A2)	563	τR$_1$(A1) R$_2$(A2)
545vw	547m	534	τR$_3$(A2)	532	τR$_3$(A2)	532	τR$_2$(A2) τR$_3$(A2)	531	τR$_2$(A2) τR$_3$(A2)
503vw	506w	501	βR$_3$(A1) βR$_2$(A2) βR$_3$(A2)	498	βR$_3$(A1) βR$_2$(A2) βR$_3$(A2)	498	βR$_3$(A1) βR$_2$(A2) βR$_3$(A2)	498	βR$_3$(A1) βR$_2$(A2) βR$_3$(A2)
454w	456vw			440	τR$_2$(A2)			442	τR$_2$(A2)
	441w	439	τR$_2$(A2)			439	τR$_2$(A2)		
413sh		418	wagCC$_2$	414	τR$_2$(A1) τR$_1$(A1)	415	τR$_2$(A1) τR$_1$(A1)	423	τR$_1$(A1) τR$_2$(A1)
413sh	404w	413	τwCC$_2$	412	τwCC$_2$	412	τR$_3$(A2) τwCC$_2$	413	τR$_3$(A2) τwCC$_2$
389m	387w	398	τR$_3$(A1)	397	τR$_3$(A1)	398	τR$_3$(A1)	399	τR$_3$(A1)
	368sh	382	δCC$_2$	381	δCC$_2$	381	δCC$_2$	384	δCC$_2$
	339sh	326	ρC3-C9 ρCC$_2$ ρ'C3-C9	325	ρC3-C9 ρCC$_2$ ρ'C3-C9	325	ρC3-C9 ρCC$_2$ρ'C3-C9	327	ρC3-C9 ρCC$_2$ ρ'C3-C9
	300w	283	τR$_1$(A1) τR$_2$(A1)	286	τR$_1$(A1) τR$_2$(A1)	286	τR$_1$(A1) τR$_2$(A1)	288	τR$_1$(A1) τR$_2$(A1)
		282	τR$_2$(A1) τR$_1$(A1)	280	τR$_2$(A1) τR$_1$(A1)	280	τR$_2$(A1) τR$_1$(A1)	284	τR$_2$(A1) τR$_1$(A1)
		242	τR$_2$(A1) τR$_1$(A1)	237	τR$_2$(A1) τR$_1$(A1)	238	τR$_2$(A1) τR$_1$(A1)	242	τR$_2$(A1) τR$_1$(A1)
		207	τwCH$_3$(C11) τwCH$_3$(C10)	218	τwCH$_3$(C11) τwCH$_3$(C10) wagCC$_2$	222	τwCH$_3$(C11) τwCH$_3$(C10) wagCC$_2$	225	τwCH$_3$(C11) τwCH$_3$(C10) wagCC$_2$
		199	τwCH$_3$(C9)	190	τR$_1$(A1)	192	τR$_1$(A1)	196	τR$_1$(A1)
		189	τR$_1$(A1)	169	τwCH$_3$(C9)	169	τwCH$_3$(C9)	175	τwCH$_3$(C9)
		154	τR$_1$(A1) R$_2$(A1)	158	τR$_1$(A1) τR$_2$(A1)	159	τR$_1$(A1) τR$_2$(A1)	164	τR$_1$(A1) τR$_2$(A1)
		45	τR$_2$(A1)	31	τR$_2$(A1)	28	τR$_2$(A1)	32	τR$_2$(A1)

Abbreviations: ν, stretching; δ, deformation in the plane; γ, deformation out of plane; wag, wagging; τ, torsion; β$_R$, deformation ring τ$_R$, torsion ring; ρ, rocking; τw, twisting; δ, deformation; a, antisymmetric; s, symmetric; (A$_1$), Ring 1; (A$_2$), Ring 2. [a]This work, [b]From scaled quantum mechanics force field, [c]From Ref [27], [d]From Ref [13].

3.7.1. Band Assignments

3.7.1.1. CH modes. Eucalyptol presents only an aliphatic C2-H12 bond for which this stretching mode can be easily assigned to the IR bands between 2946 and 2885 because the calculations in all media are predicted in this region. The two C-H rocking modes expected for this group are predicted by SQM calculations coupled with some wagging and twisting modes of CH_2 groups and, also with a torsion R2 ring mode in the 1344-1205 cm^{-1} region, as detailed in Table 8. Hence, these modes can be assigned to the IR and Raman bands between 1339 and 1211 cm^{-1}.

3.7.1.2. CH_3 modes. Eucalyptol has three CH_3 groups and, hence, nine stretching modes are expected for each group. The detailed assignments presented in Table 8 show that the antisymmetric stretching modes are predicted at higher wavenumbers between 3013 and 2980 cm^{-1} while the symmetrical stretching modes between 2932 and 2921 cm^{-1}. Hence, they can be assigned in the regions predicted by SQM calculations. Obviously, the symmetries of these modes cannot be confirmed because the experimental Raman was recorded between 2000 and 300 cm^{-1}. In alkaloids species and cyclizine, the antisymmetric and symmetric deformation modes are assigned between 1472 and 1398 cm^{-1} [41-43,45] and, in eucalyptol, these modes are predicted in all media between 1463 and 1351 cm^{-1} and, for these reasons, the IR and Raman bands in these regions can be assigned to those vibration modes. The rocking modes are normally assigned between 1200 and 1011 cm^{-1} while the twisting modes between 259 and 204 cm^{-1} [30,32,33,35-45]. In eucalyptol, those modes are predicted between 1236/990 and 225/169 cm^{-1}, respectively. Hence, only the rocking modes are assigned in the expected regions but the twisting modes were not assigned because the experimental Raman was recorded up to 300 cm^{-1}.

3.7.1.3. CH_2 modes. In alkaloids and cyclizine species, the antisymmetric and symmetric stretching modes are assigned between 3037 and 2793 cm^{-1} [41-43,45]. In eucalyptol, the antisymmetric and symmetric stretching modes of four CH_2 groups are predicted in the 2981-2919 cm^{-1} region. Therefore, these vibration modes can be attributed to the IR and Raman bands observed in that region. The deformation and wagging modes in cocaine and tropane are respectively predicted at 1483/1442 and 1382/1242 cm^{-1} [41-43] while in eucalyptol in the four media are predicted between 1492/1424 and 1380/1321 cm^{-1}. Hence, the bands observed in both spectra en these regions can be assigned to those two vibration modes. The rocking and twisting modes in cocaine and tropane are predicted respectively at 1274/1142 and 967/639 cm^{-1} while in cyclizine those two modes are assigned at 1319/1203 and 1037/766 cm^{-1} [45]. For these reasons, in eucalyptol, these two rocking and twisting modes are assigned as predicted by calculations between 1282/1098 and 773/730 cm^{-1}.

3.7.1.4. Skeletal modes. For eucalyptol in the four media, the two O1-C3 and O1-C4 stretching modes are predicted practically in the same regions, thus, that first mode is predicted between 973 and 950 cm^{-1} while the second one is predicted between 819 and 810 cm^{-1}. These two modes are slightly influenced by the medium because in water both stretching modes are shifted toward lower wavenumbers due probably to the hydration with water molecules. The three C-CH_3 stretching modes (C3-C9, C4-C10, and C4-C11) are predicted in the gas phase in regions different from the three solutions, hence, the C3-C9 stretching modes are predicted between 1152 and 1158 cm^{-1} while the other two between 913 and 909 cm^{-1}. Consequently, those stretching modes are assigned to the IR and Raman bands observed between 1163 and 920 cm^{-1}, as observed in Table 8. The remain skeletal vibration modes together with the deformations and torsion rings are assigned considering the SQM calculations and the assignments for similar species [30,32,34-45], as shown in Table 8.

4. Force constants

For eucalyptol in the four media were calculated the harmonic force constants by using the corresponding harmonic force fields with the B3LYP/6-31G* method. Here, the SQMFF procedure and suitable scale factors [26,58] were employed together with the Molvib program [26] to obtain the scaled harmonic force fields. In **Table 9** are shown the main force constants for eucalyptol in the different media.

Table 9. Scaled internal force constants for eucalyptol in different media by using the B3LYP/6-31G* method.

Force constant	Eucalyptol[a]			
	Gas	Chloroform	Acetone	Water
$f(\nu C\text{-}H)$	4.74	4.76	4.76	4.77
$f(\nu C\text{-}O)$	4.22	4.09	4.09	3.92
$f(\nu CH_2)$	4.79	4.79	4.79	4.80
$f(\nu CH_3)$	4.89	4.87	4.87	4.88
$f(\nu C\text{-}CH_3)$	3.92	3.92	3.92	3.94
$f(\delta CH_2)$	0.74	0.73	0.73	0.73
$f(\delta CH_3)$	0.55	0.54	0.54	0.54

Units are mdyn $Å^{-1}$ for stretching and mdyn Å rad^{-2} for angle deformations

[a]This work

The results show practically similar values in all media but, particularly in water are observed slight differences in some values, as compared with the values in the gas phase. Here, the *f(νC-O)* force constant shows the lower value in water because this region is strongly nucleophilic, as revealed by the mapped MEP surface and, taking into account the higher permittivity of water this region is the site of higher hydration. The higher dipole moment and corrected solvation energy values observed in this medium together with the lower volume value support clearly the higher hydration in water. Evidently, the similarities in the other force constants show that they are not influenced by the characteristic of the solvent.

5. Ultraviolet-visible spectrum

The UV-visible spectra of eucalyptol in water, acetone, and chloroform solutions were predicted by using Time-dependent DFT calculations (TD-DFT) with the B3LYP/6-31G* method and the Gaussian 09 program [49]. These spectra were compared in **Figure 9** with that experimental reported for eucalyptol standard by Alam et al [7].

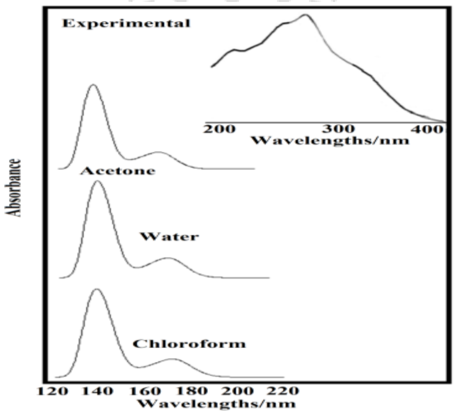

Figure 6. Experimental UV-visible of eucalyptol compared with the corresponding predicted in acetone, water, and chloroform solutions by using B3LYP/6-31G* level of theory.

These studies are very important taking into account that Lee et al have reported that eucalyptol or 1,8-cineole prevents UVB-induced skin carcinogenesis by targeting the aryl hydrocarbon receptor [2]. The experimental spectrum shows a maximum in c.a. 280 nm with two shoulders in approximately 220 and 300 nm while in the predicted spectra can be observed two bands, an intense in c.a. 140 and the other one less intense at 175 nm. The theoretical UV spectra of eucalyptol in the different solvents show slight variations only in the intensities of the most intense band located at 140 nm. These bands could be associated with those two $\Delta E_{\sigma\rightarrow\sigma^*}$ and $\Delta E_{n\rightarrow\sigma^*}$ transitions predicted for eucalyptol in different media by using NBO calculations. Note that in the experimental spectrum these bands are not observed because the UV-visible spectrum was recorded from 200 to 400 nm.

6. NMR studies

In **Tables 10** and **11** are presented the predicted ^{1}H and ^{13}C NMR chemical shifts of eucalyptol in different media calculated by using the GIAO method [55] and the hybrid B3LYP/6-31G* method with the corresponding experimental available ^{1}H and ^{13}C NMR spectra of eucalyptol in $CDCl_3$ taken from Ref [59,60]. We observed that there are overestimations of calculated values in relation to the experimental ones and a better correlation is found for the ^{1}H nucleus with an RMSD value of 0.4 ppm in all media. The calculations for the ^{13}C nucleus show a better correlation with the values taken from Ref [59] than those experimental reported from Ref [60], thus, the RMSD values are in the first case between 6.3 and 6.2 while in the second one the values change between 6.9 and 6.7 ppm. These values are very good considering that the calculations were performed by using the 6-31G* basis set instead of the 6-311++G** basis set, as recommended mainly for the H nuclei where better results are obtained with the higher size basis set. At this point, the same RMSD values obtained for eucalyptol in all media do not show changes in solution in relation to the values in the gas phase.

Table 10. Observed and calculated ^{1}H chemical shifts (δ in ppm) for eucalyptol in different media by using the B3LYP/6-31G* method.

	Eucalyptol[a]				Exp[b]
H atom	Gas	Chloroform	Acetone	Water	
12-H	1.18	1.16	1.15	1.14	1.416
13-H	1.84	1.84	1.84	1.83	2.031
14-H	1.22	1.22	1.21	1.20	1.506
15-H	1.22	1.22	1.21	1.20	1.506
16-H	1.84	1.84	1.84	1.83	2.031
17-H	1.24	1.23	1.23	1.21	1.506
18-H	1.43	1.45	1.45	1.45	1.675
19-H	1.43	1.45	1.45	1.45	1.506
20-H	1.24	1.23	1.23	1.21	2.031
21-H	0.48	0.47	0.47	0.45	1.061
22-H	0.83	0.85	0.86	0.86	1.061
23-H	0.83	0.85	0.86	0.86	1.061
24-H	0.54	0.55	0.55	0.52	1.249
25-H	0.96	0.99	0.99	1.00	1.249
26-H	1.24	1.26	1.26	1.27	1.249
27-H	0.54	0.55	0.55	0.52	1.249
28-H	1.24	1.26	1.26	1.27	1.249
29-H	0.96	0.99	0.99	1.00	1.249
RMSD	**0.4**	**0.4**	**0.4**	**0.4**	

[a]This work GIAO/B3LYP/6-31G* Ref. to TMS, [b]From Ref [59]

Table 11. Observed and calculated ^{13}C chemical shifts (δ in ppm) for eucalyptol in different media by using the B3LYP/6-31G* method.

	Eucalyptol[a]				Exp[b]	Exp[c]
C atoms	Gas	Chloroform	Acetone	Water		
2-C	27.22	27.28	27.36	27.33	32.94	33.456
3-C	61.98	62.36	62.36	62.90	69.77	70.337
4-C	66.05	66.31	66.31	66.86	73.61	74.178
5-C	19.05	19.04	19.02	18.89	22.83	23.361
6-C	19.05	19.03	19.02	18.88	22.83	23.361
7-C	25.54	25.55	25.58	25.44	31.51	32.034
8-C	25.54	25.55	25.58	25.44	31.51	32.034
9-C	20.70	20.65	20.66	20.54	27.58	28.127
10-C	21.67	21.70	21.74	21.62	28.88	29.431
11-C	21.67	21.69	21.74	21.62	28.88	29.431
RMSD[b]	**6.3**	**6.3**	**6.2**	**6.2**		
RMSD[c]	**6.9**	**6.8**	**6.8**	**6.7**		

[a]This work GIAO/B3LYP/6-31G* Ref. to TMS, [b]From Ref [59],[c]From Ref [60]

7. Lapinski's and Veber's criteria

In this work, the pharmacological properties of eucalyptol were evaluated according to the Lapinski's and Veber's criteria [46,47]. Hence, eucalyptol could present absorption or permeation because only three of the four criteria were found, (i) there is not donor groups in eucalyptol (< number than 5 H-bond donors), (ii) the molecular weight (MWT) is <<< than 500 and, (iii) eucalyptol shows only an H-bond acceptor O atom (< 10 H-bond acceptor). Therefore, eucalyptol could present pharmacological properties.

CONCLUSIONS

Eucalyptol has been studied theoretically in the gas phase and in acetone, chloroform, ethanol, and water solutions by using the hybrid B3LYP/6-31G* level of theory. Here, the SCRF and PCM methods were used together with the universal solvation model to study the properties in different solvents. The properties were evaluated in function of the solvent's permittivities. The optimization only for eucalyptol in ethanol solution has evidenced an imaginary frequency. A higher dipole moment and lower volume values for eucalyptol were observed in water due probably to the higher permitivity. Also, higher corrected solvation energy is predicted for eucalyptol in water (-22.51 kJ/mol) in agreement with the higher volume contraction observed in this medium (-0.4 Å^3). Probably, the higher hydration of eucalyptol in water and the H bonds formation could justify these observations. The studies of atomic charges reveal that on the O atoms are observed the most negative MK, Mulliken and NPA charges while the most positive values are observed on the C3 and C4 atoms.

The mapped MEP surfaces of eucalyptol in the different media have evidenced clearly nucleophilic sites located on the O atoms.

The NBO analyses show practically the same stabilities in all media due to the two $\Delta E_{\sigma\rightarrow\sigma^*}$ and $\Delta E_{LP\rightarrow\sigma^*}$ transitions while the AIM studies reveal two H---H interactions which support the stabilities of eucalyptol in all studied media.

The studies of frontier orbitals evidence that the presence of an O atom linked to a bicyclic ring in eucalyptol increase the gap values and decreasing the reactivities of eucalyptol in the gas phase and mainly in chloroform and acetone solutions while in aqueous solution eucalyptol is slightly most reactive. Besides, these frontier orbitals studies support the characteristics of eucalyptol as a powerful nucleophile against reacting with potential biological electrophiles.

The harmonic force fields of eucalyptol in all media were calculated with the SQMFF methodology and the Molvib program. Then, the complete vibrational assignments of 81 normal vibration modes for eucalyptol in all media were performed by using the normal internal coordinates and the experimental available IR, ATR and Raman spectra. Additionally, the force constants were also reported for first time.

The predicted IR, ATR, Raman, ^{1}H- and ^{13}C-NMR and UV-visible spectra show reasonable concordance with the corresponding experimental ones.

Data Availability

The SQM force fields for eucalyptol in all solvents can be obtained at request.

Conflicts of Interest

Authors declare there are not a conflict of interests.

Funding Statement

This work was supported with grants from CIUNT Project Nº 26/D608 (Consejo de Investigaciones, Universidad Nacional de Tucumán).

ACKNOWLEDGMENTS

The authors would like to thank Prof. Tom Sundius for his permission to use MOLVIB.

REFERENCES

[1] Leighton X Bera A, Eidelman O, Eklund M, Puthillathu N, Pollard HB, Srivastava M. High ANXA7 Potentiates Eucalyptol Toxicity in Hormone-refractory Prostate Cancer. Anticancer Research, 2018, 38: 3831-3842.

[2] Lee J, Ha SJ, Park J, Kim YH, Lee NH, Kim YE, Kim Y, Song K-M, Jung SK. 1,8-cineole prevents UVB-induced skin carcinogenesis by targeting the aryl hydrocarbon receptor. Oncotarget, 2017, 8(62): 105995-106008.

[3] Hąc-Wydro K, Blecharz A, Wydro P. The influence of eucalyptol/terpinen-4-ol mixtures on monolayers imitating plant pathogen Botrytis cinerea membranes. J. Mol. Liq. 2018, 271: 472-480.

[4] Collis GE, Unterweger B, Dumsday GJ, Forsyth CM. Structural elucidation of a hydroxy–cineole product obtained from cytochrome P450 monooxygenase CYP101J2 catalyzed the transformation of 1,8-cineole. Acta Cryst. 2017, E73: 1242–1245.

[5] Bounaas K, Bouzidi N, Daghbouche Y, Garrigues S, de la Guardia M, El Hattab M. Fourier transform infrared analysis of commercial formulations for Varroa treatment. Anal. Methods, 2017, 9: 6574-6582.

[6] Hąc-Wydro K, Flasiński M, Broniatowski M, Sołtys M. Studies on the Behavior of Eucalyptol and Terpinen-4-ol-Natural Food Additives and Ecological Pesticides-in Model Lipid Membranes. Langmuir, 2017, 33(27): 6916–6924.

[7] Alam P, Alqasoumi SI, Abdel-Kader MS. Simultaneous Determination of Menthol and Eucalyptol by the Densitometric HPTLC Method in Some External Analgesic Formulations. J. Chromatographic Science, 2016, 54(1): 58–63.

[8] Ribeiro DA, Alencar Marques ME, Fávero Salvador DM. In Vitro Cytotoxic and Non-Genotoxic Effects of Gutta-Percha Solvents on Mouse Lymphoma Cells by Single Cell Gel (Comet) Assay. Braz. Dent. J. 2006, 17(3): 228-232.

[9] Juergens UR, Stöber M, Vetter H. Inhibition of cytokine production and arachidonic acid metabolism by eucalyptol (1.8-cineole) in human blood monocytes in vitro. Eur J Med Res. 1998; 3: 508-10.

[10] Wang Y. Inhibitory effect of 1, 8-cineol (eucalyptol) on Egr-1 expression in lipopolysaccharide-stimulated THP-1 cells. Acta Pharmacol Sin. 2007; 28: 908-12.

[11] Bastos VP, Gomes AS, Lima FJ, Brito TS, Soares PM, Pinho JP, Silva CS, Santos AA, Souza MH, Magalhães PJ. Inhaled 1, 8-cineole reduces inflammatory parameters in airways of ovalbumin-challenged Guinea pigs. Basic Clin Pharmacol Toxicol. 2011; 108: 34-39.

[12] Lima PR, de Melo TS, Carvalho KM, de Oliveira ÍB, Arruda BR, de Castro Brito GA, Rao VS, Santos FA. 1, 8-cineole (eucalyptol) ameliorates cerulein-induced acute pancreatitis via modulation of cytokines, oxidative stress and NF-κB activity in mice. Life Sci. 2013; 92: 1195-201.

[13] Hartwig Schulz MB, Walter A, Rösch P, Quilitzsch R, Lösing G, Popp J., Investigation of eucalyptus essential oil by using vibrational spectroscopy methods. Vibrational Spectroscopy, 2006, 42: 341–345.

[14] Baranska M, Schulz H, Reitzenstein S, Uhlemann U, Strehle MA, Krüger H, Quilitzsch R, Foley W, Popp J. Vibrational Spectroscopic Studies to Acquire a Quality Control Method of Eucalyptus Essential Oils, Quality Control of Eucalyptus. Essential Oils, 2005, 237-248.

[15] Hameed IH, Ibraheam IA, Kadhim HJ. Gas chromatography-mass spectrum and Fourier transform infrared spectroscopy analysis of a methanolic extract of Rosmarinus Officinalis leaves. Journal of Pharmacognosy and Phytotherapy, 2015, 7(6): 90-106.
[16] Lafhal S, Vanloot P, Bombarda I, Valls R, Kister J, Dupuy N. Raman spectroscopy for identification and quantification analysis of essential oil varieties: a multivariate approach applied to lavender and lavandin essential oils. J. Raman Spectroscopy, 2015, 46(6): 577-585.
[17] Raveendran P, Zimmermann D, Häber T, Suhm MA. Exploring a hydrogen-bond terminus: spectroscopy of eucalyptol–alcohol clusters. Phys. Chem. Chem. Phys. 2000, 2: 3555-3563.
[18] Daferera DJ, Tarantilis PA, Polissiou MG. Characterization of essential oils from Lamiaceae species by fourier transform Raman spectroscopy, J Agric Food Chem. 2002, 50(20): 5503-7.
[19] Barnes JC, Quinol-1,8-Epoxymenthane (1 2). Acta Cryst. 1988, C44: 118-120.
[20] Becke AD. Density-functional exchange-energy approximation with correct asymptotic behavior, Phys. Rev. 1988, A38: 3098-3100.
[21] Lee C, Yang W, Parr RG. Development of the Colle-Salvetti correlation-energy formula into a functional of the electron density. Phys. Rev. 1988, B37: 785-789.
[22] Miertus S, Scrocco E, Tomasi J. Electrostatic interaction of a solute with a continuum. Chem**.** Phys**.** 1981, 55: 117**–**129.
[23] Tomasi J, Persico J. Molecular Interactions in Solution: An Overview of Methods Based on Continous Distributions of the Solvent. Chem. Rev. 1994, 94: 2027-2094.
[24] Marenich AV, Cramer CJ, Truhlar DG. Universal solvation model based on solute electron density and a continuum model of the solvent defined by the bulk dielectric constant and atomic surface tensions. J. Phys. Chem. 2009, B113: 6378-6396.
[25] Pulay P, Fogarasi G, Pongor G, Boggs JE, Vargha A. Combination of theoretical ab initio and experimental information to obtain reliable harmonic force constants. Scaled quantum mechanical (QM) force fields for glyoxal, acrolein, butadiene, formaldehyde, and ethylene, J. Am. Chem. Soc. 1983, 105: 7073.
[26] Sundius T. Scaling of ab-initio force fields by MOLVIB, Vib. Spectrosc. 2002, 29: 89-95.
[27] Infrared Spectrum of 2-Oxabicyclo[2.2.2]octane in the gas phase. Available from: https://webbook.nist.gov/cgi/cbook.cgi?ID=C470826&Type=IR-SPEC&Index=0#IR-SPEC.
[28] Parr RG, Pearson RG. Absolute Hardness: companion parameter to absolute electronegativity, J. Am. Chem. Soc. 1983, 105: 7512-7516.
[29] J-L Brédas, Mind the gap!, Materials Horizons, 2014, 1: 17–19.
[30] Romani D, Brandán SA, Márquez MJ, Márquez MB. Structural, topological and vibrational properties of an isothiazole derivatives series with antiviral activities. J. Mol. Struct. 2015, 1100: 279-289.
[31] Romani D, Tsuchiya S, Yotsu-Yamashita M, Brandán SA. Spectroscopic and structural investigation on intermediates species structurally associated with the tricyclic bisguanidine compound and to the toxic agent, saxitoxin. J. Mol. Struct. 2016, 1119: 25-38.
[32] Romano E, Castillo MV, Pergomet JL, Zinczuk J, Brandán SA. Synthesis, structural and vibrational analysis of (5,7-Dichloro-quinolin-8-yloxy) acetic acid. J. Mol. Struct. 2012, 1018: 149–155.
[33] Iramain MA, Davies L, Brandán S.A. Structural and spectroscopic differences among the Potassium 5-hydroxypentanoyltrifluoroborate salt and the furoyl and isonicotinoyl salts. J Mol. Struct. 2019, 1176: 718-728.
[34] Issaoui N, Ghalla H, Brandán SA, Bardak F, Flakus HT, Atac A, Oujia B. Experimental FTIR, and FT-Raman and theoretical studies on the molecular structures of monomer and dimer of 3-thiopheneacrylic acid. J. Mol. Struct. 2017, 1135: 209-221.
[35] Minteguiaga M, Dellacassa E, Iramain MA, Catalán CAN, Brandán SA. FT-IR, FT-Raman, UV-Vis, NMR and structural studies of Carquejyl Acetate, a component of the essential oil from *Baccharis trimera* (Less.) DC. (Asteraceae). J Mol. Struct. 2018, 1177: 499-510.
[36] Minteguiaga M, Dellacassa E, Iramain MA, Catalán CAN, Brandán SA. A structural and spectroscopic study on carquejol, a relevant constituent of the medicinal plant Baccharis trimera (Less.) DC. (Asteraceae). J. Mol. Struct. 2017, 1150: 8-20.
[37] Chain F, Ladetto MF, Grau A, Catalán CAN, Brandán SA. Structural, electronic, topological and vibrational properties of a series of N-benzylamides derived from Maca (*Lepidium meyenii*) combining spectroscopic studies with ONION calculations. J. Mol. Struct. 2016, 1105: 403-414.

[38] Chain F, Romano E, Leyton P, Paipa C, Catalán CAN, Fortuna MA, Brandán SA. Vibrational and structural study of onopordopicrin based on the FTIR spectrum and DFT calculations, Spectrochim. Acta, 2015, 150: 381-389.

[39] Chain F, Romano E, Leyton P, Paipa C, Catalán CAN, Fortuna MA, Brandán SA. An experimental study of the structural and vibrational properties of sesquiterpene lactone cnicin using FT-IR, FT-Raman, UV–visible and NMR spectroscopies. J. Mol. Struct. 2014, 1065-1066: 160-169.

[40] Chain FE, Leyton P, Paipa C, Fortuna M, Brandán SA. FT-IR, FT-Raman, UV-Visible, and NMR spectroscopy and vibrational properties of the labdane-type diterpene 13-epi-sclareol. Spectrochim. Acta Part A, 2015, 138: 303-313.

[41] Rudyk RA, Brandán SA. Force field, internal coordinates and vibrational study of alkaloid tropane hydrochloride by using their infrared spectrum and DFT calculations. Paripex A Indian Journal of Research, 2017, 6(8): 616-623.

[42] Romani D, Brandán SA. Vibrational analyses of alkaloid cocaine as free base, cationic and hydrochloride species based on their internal coordinates and force fields. Paripex A Indian Journal of Research, 2017, 6(9): 587-602.

[43] Rudyk RA, Checa MA, Catalán CAN, Brandán SA. Structural, FT-IR, FT-Raman and ECD spectroscopic studies of free base, cationic and hydrobromide species of scopolamine alkaloid. J. Mol. Struct. 2019, 1180: 603-617.

[44] Iramain MA, Brandán SA. Structural and vibrational properties of three species of anti-histaminic diphenhydramine by using DFT calculations and the SQM approach. To Chemistry Journal, 2018, 1(1): 105-130.

[45] Márquez MJ, Iramain MA, Brandán SA. *Ab-initio* and Vibrational studies on Free Base, Cationic and Hydrochloride Species Derived from Antihistaminic Cyclizine agent. IRM, International Journal of Science and Research Methodology, 2018, 12(2): 97-140.

[46] Lipinski CA, Lombardo F, Dominy BW, Feeney PJ. Experimental and computational approaches to estimate solubility and permeability in drug discovery and development settings. Adv Drug Deliv Rev. 2001, 46(1-3): 3-26.

[47] Veber DF, Johnson SR, Cheng HY, Smith BR, Ward KW, Kopple KD. Molecular properties that influence the oral bioavailability of drug candidates. J Med Chem. 2002, 45(12): 2615-23.

[48] Nielsen AB, Holder AJ. Gauss View 3.0, User's Reference, GAUSSIAN Inc., Pittsburgh, PA, 2000–2003.

[49] Frisch MJ, Trucks GW, Schlegel HB, Scuseria GE, Robb MA, Cheeseman JR, Scalmani G, Barone V, Mennucci B. Petersson GA, Nakatsuji H, Caricato M, Li X, Hratchian HP, Izmaylov AF, Bloino J, Zheng G, Sonnenberg JL, Hada M, Ehara M, Toyota K, Fukuda R, Hasegawa J, Ishida M, Nakajima T, Honda Y, Kitao O, Nakai H, Vreven T, Montgomery JA, Peralta JE, Ogliaro F, Bearpark M, Heyd JJ, Brothers E, Kudin KN, Staroverov VN, Kobayashi R, Normand J, Raghavachari K, Rendell A, Burant JC, Iyengar SS, Tomasi J, Cossi M, Rega N, Millam JM, Klene M, Knox JE,. Cross JB, Bakken V, Adamo C, Jaramillo J, Gomperts R, Stratmann RE, Yazyev O, Austin AJ, Cammi R, Pomelli C, Ochterski JW, Martin RL, Morokuma K, Zakrzewski VG, Voth GA, Salvador P, Dannenberg JJ, Dapprich S, Daniels AD, Farkas O, Foresman JB, Ortiz J., Cioslowski J, Fox DJ. Gaussian, Inc., Wallingford CT, 2009.

[50] Ugliengo P. Moldraw Program, University of Torino, Dipartimento Chimica IFM, Torino, Italy, 1998.

[51] Besler BH, Merz Jr KM, Kollman PA. Atomic charges derived from semiempirical methods, J. Comp. Chem. 1990, 11: 431-439.

[52] Glendening ED, JBadenhoop. K, Reed AD, Carpenter JE, Weinhold F. NBO 3.1; Theoretical Chemistry Institute, University of Wisconsin; Madison, WI, 1996.

[53] Bader RFW. Atoms in Molecules, A Quantum Theory, Oxford University Press, Oxford, 1990, ISBN: 0198558651.

[54] Biegler-Köning F, Schönbohm J, Bayles D. AIM2000; A Program to Analyze and Visualize Atoms in Molecules. J. Comput. Chem. 2001, 22: 545.

[55] Ditchfield R. Self-consistent perturbation theory of diamagnetism. I. A gage-invariant LCAO (linear combination of atomic orbitals) method for NMR chemical shifts. Mol Phys. 1974, 27: 714–722.

[56] Keresztury G, Holly S, Besenyei G, Varga J, Wang AY, Durig JR. Vibrational spectra of monothiocarbamates-II. IR and Raman spectra, vibrational assignment, conformational analysis and ab initio calculations of S-methyl-N, N-diethyldithiocarbamate. Spectrochim. Acta, 1993, 49A: 2007-2026.

[57] Michalska D, Wysokinski R. The prediction of Raman spectra of platinum(II) anticancer drugs by density functional theory. Chem. Phys. Lett. 2005, 403: 211-217.

[58] a) Rauhut G, Pulay P, Transferable Scaling Factors for Density Functional Derived Vibrational Force Fields, J. Phys. Chem. 1995, 99: 3093-3100. b) *Correction:* G. Rauhut, P. Pulay, J. Phys. Chem. 1995, 99: 14572.

[59] Experimental ^{1}H- and ^{13}C-NMR spectra of eucalyptol in $CDCl_3$ by Madison Metabolomics Consortium - Francisca Jofre, Mark E. Anderson, John L. Markley.

[60] ^{1}H- and ^{13}C-NMR spectra of eucalyptol available from downloads.hindawi.com/journals/jchem/2015/549057.f1.pdf.